New strategy of solid/fluid coupling during numerical simulation of thermo-mechanical processes

Yassine Saadlaoui, Alexandre Delache, Eric Feulvarch, Jean-Baptiste B Leblond, Jean-Michel Bergheau

New strategy of solid/fluid coupling during numerical simulation of thermo-mechanical processes

Y. Saadlaoui[a,*], A. Delache[b], E. Feulvarch[a], J.B. Leblond[c], J.M. Bergheau[a]

[a] *Univ Lyon, ENISE, LTDS, UMR 5513 CNRS, 58 rue Jean Parot, 42023 Saint-Etienne Cedex 02, France*
[b] *Univ Lyon, UJM, LMFA, UMR 5509 CNRS, Saint-Étienne, France*
[c] *UPMC, Univ Sorbonne, Institut Jean-Le-Rond-d'Alembert, UMR 7190, Tour 65–55, 4, place Jussieu, 75252 Paris cedex 05, France*

Abstract

In this study, numerical methods are developed to simulate thermomechanical processes, taking into account both the fluid flows in the molten pool and the deformations of the solid parts. The methods are based on a new strategy of solid/fluid coupling. They allow to simulate the formation of the molten pool by taking into account the fluid flows through both effects of the surface tension ("curvature effect" and "Marangoni effect") and the buoyancy. An ALE approach is used to follow the evolution of the free surface. The effects of the deformations in the base metal on the fluid flows in the molten pool (solid/fluid interaction) is ensured by imposing the velocities of the solid nodes during the thermo-fluid simulation. As an application, a thermo-fluid-mechanical simulation of laser welding is carried out. It is found that the solid/fluid interaction has a minor effect on simulation results.

Keywords: Solid/Fluid interaction, Fluid flows, Solid deformations, Thermo-mechanical processes, Numerical simulation.

1. Introdution

The welding process was invented in the late 19th-century to replace the riveting assembly process used at the time. The techniques used for the welding process have evolved considerably: the first technique consisted of assembling parts by heating and hammering, then by arc welding and resistance

*Corresponding author
Email addresses: yassine.saadlaoui@enise.fr (Y. Saadlaoui), jean-michel.bergheau@enise.fr (J.M. Bergheau)

welding. During the 20th-century, new techniques were developed that rely on electron and laser beams. These assembly techniques are multi-physical processes that involve high temperatures and whose metallurgical and mechanical consequences must be controlled in order to ensure a good quality (strain, residual stresses, lifetime, etc.) of assembled parts. Several experimental studies have shown that the final characteristics of these parts are very sensitive to welding parameters. The optimization of these parameters is therefore an essential step in obtaining high quality parts. Experimental tests can be used as a means of optimization. However, they are generally long to be carried out and very expensive. In this context, the numerical simulation is of special interest for optimizing the process parameters, and for predicting the final characteristics of the welded parts with a reasonable cost and computation time.

Several numerical methods have been developed to simulate the welding techniques [1, 2, 3, 4, 5, 6, 7, 8, 9, 10]. The thermo-mechanical simulation consists in performing a thermal calculation and a mechanical calculation taking the thermal results as input. The thermal simulation most often does not take account of the fluid flows in the molten pool in order to reduce the computation time. Nowadays, this type of simulation is well-used in industrial companies. It allows to estimate the metallurgical and mechanical consequences induced by welding (microstructure, residual stresses and distortions)[1, 2, 11, 12, 13, 14, 15, 16, 17, 18], thus providing very relevant information for the quality of the final structure and for fatigue lifetime predictions.

However, this kind of simulation is not completely predictive as, because fluid flows in the melted pool are neglected, a careful calibration of the heat input to get good temperature distributions is required. Indeed, different researches show that the fluid flows have major direct effects on the morphology of the molten pool and on the temperature distributions [19, 20, 21]. For example, according to the sign of the surface tension gradient, the molten pool morphology can be completely different [20, 22, 23]. Indeed, the molten pool is longer and shallower in the case of a negative gradient $\frac{\partial \gamma}{\partial T} < 0$. It is well-known that the molten zone morphology, in turn, affects the residual stress and distortion. Thus, the mechanical computation can be sensitive to fluid flows. At the same time, the deformations of the base metal also lead to a change of the morphology of the molten pool, which thus modifies the flows in the molten metal (figure 1). This is why the interaction between the fluid flows and the solid deformations is a strong interaction. Here, the problem is that the fluid and the solid computations are usually simulated separately, with very few interactions between them. Generally, only the effect of the thermo-fluid simulation on the solid computation is taken into

account through the thermal cycle.

Some studies have been conducted to simulate the interaction between the fluid and the solid. Generally, a weak coupling is used [24, 25]. It consists in starting with a thermal-fluid simulation, which will give the temperature evolution over time. The temperature fields thus determined are then applied as loading, so that a mechanical simulation will determine the fields of stresses and deformations [2, 24, 26]. However, the effect of the solid deformations on the fluid flows is neglected in the thermo-fluid simulation. Neglecting this effect can impact first the thermo-fluid results (temperature, flows velocity, morphology of the molten pool, etc.) and thereafter the mechanical results.

Some authors have developed other approaches to simulate this interaction in a more physical way. These approaches consist in using a strong coupling to calculte the fluid flows and the solid deformations [27, 28].

These numerical simulations, which use an implicit algorithm remain very rare. For example, Heuzé et al. [27] have successfully implemented a strong coupling to simulate the Friction Stir Spot Welding process where the stirred zone is modeled as a non-Newtonian fluid. For this process, the behavior of the fluid (stirred) zone is quite close to that of a solid. However, the use of that type of coupling for high-temperature processes (laser welding, additive manufacturing processes, etc.), where the melting temperature is widely exceeded and the molten zone behaves as a Newtonian fluid, poses several numerical problems [28] coming from:

- the mechanical characteristics: the huge difference in mechanical characteristics between the fluid and the solid can generate an impossibility of convergence of the nonlinear algorithm.
- the type of the approaches: Lagrangian for the solid and Eulerian for the fluid.
- the finite elements: the different behaviors of the solid and fluid phases (in particular the quasi-incompressibility of the fluid phase, as opposed to the compressibility of the solid phase) require different numerical formulations.
- the time step and the mesh: the fluid requires a refined mesh and a smaller time step compared to those of the solid.

These points of divergence between the fluid and solid states make the simulation of the strong coupling with an implicit algorithm an almost impossible task [28].

In this context, the aim of this paper is to propose efficient numerical methods (good convergence, reasonable computation time) to simulate the couplings between the fluid flows in the molten zone and the deformations of the solid parts. The formulation of the fluid problem developed by Saadlaoui et al. [21] is used to simulate the fluid flows in the molten pool. It allows to take into account the surface tension (including both the "curvature effect" and the "Marangoni effect" [29]), buoyancy forces, and the free surface motion. The originality of this formulation remains its simplicity, its efficiency, and especially its computation time, which is very reasonable. Saadlaoui et al. [21] have simulated the sloshing problem [30] (it consists in following the oscillations of a liquid in a container) to validate this fluid formulation. They have used a spatial discretization eight times larger and a time step five times greater than those used by previous studies [31]. For those reasons, this fluid formulation will allow us to minimize the time cost and to use the same mesh for thermo-fluid and mechanical simulations.

However, Saadlaoui et al. [21] did not consider the solid/fluid interaction. In contrast, the originality of the proposed study lies in the development of a new strategy of solid/fluid coupling. It allows to simulate the interaction between the fluid flows in the molten pool and the solid deformations in the base metal. It consists in taking into account the effect of the solid deformations on the fluid flows by imposing solid velocities during the thermo-fluid computation. These solid velocities arise at each time step from a solid computation (mechanical computation). Note that the thermo-fluid and solid computations are based separately on implicit schemes. Then, these two computations are strongly coupled, which means that one influences the other, and vice versa. However, this strong coupling is carried out with an explicit algorithm. This means that the thermo-fluid computation at time $t + \Delta t$ affects the solid computation at the same instant. In contrast, the solid simulation at time $t + \Delta t$ influences the thermo-fluid computation at the following instant: $t + 2\Delta t$ (we do not iterate on the thermo-fluid and solid computations at time $t + \Delta t$: explicit algorithm).

The paper is organized as follows:

- in section 2, the proposed strategy of the solid/fluid interaction (strong coupling with an explicit algorithm) is presented. It contains three parts: an explanation of the principle of this strategy, the procedure of the solid/fluid coupling, and the constitutive laws of the different zones (fluid, mushy, and solid zones).
- in section 3, an application to the simulation of laser welding by conduction (without keyhole formation) is presented. It will allow us to test the new strategy of solid/fluid coupling. Of course, this new strategy can be used during the simulation of other thermo-mechanical processes (other welding techniques, additive manufacturing processes, etc.).

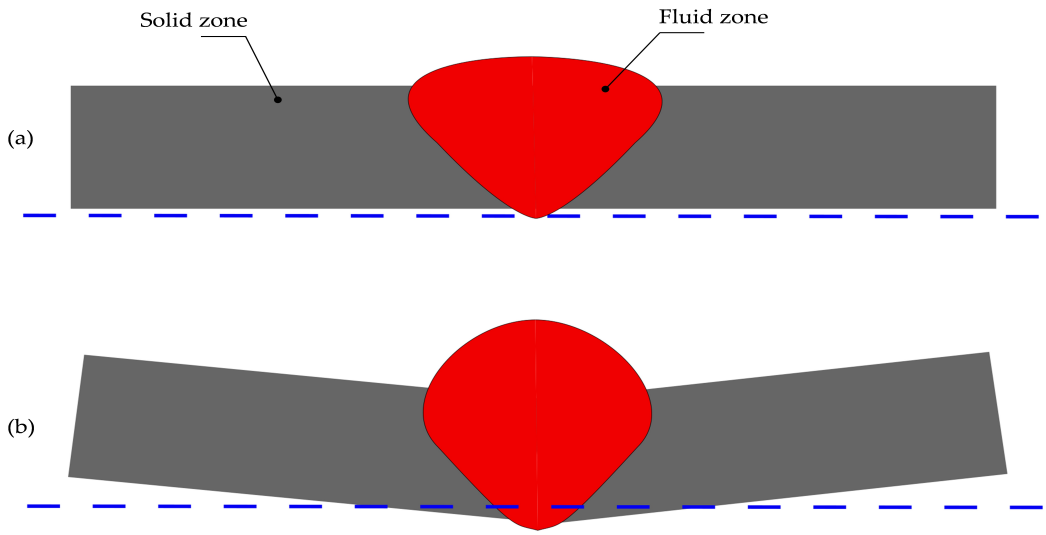

Figure 1: Schematic view of the effect of solid on fluid : (a) initial morphology of molten pool; (b) effect of the solid deformations on the morphology of molten pool.

2. Modeling of the solid/fluid interaction

2.1. Principe of the proposed strategy

Several authors have shown that the fluid flows have a great effect on the temperature field [21, 28, 32]. For example, Saadlaoui et al. [21] have compared the temperature distributions resulting from a thermo-fluid simulation (thermal with fluid flows) and another purely thermal simulation (thermal without fluid flows). They have noted a significant temperature

drop given by the thermo-fluid simulation. This temperature drop is related to the convection in the molten pool which is neglected in the purely thermal simulation. As a consequence, the fluid flows also affect the solid simulation (the action of fluid on solid), the results of which strongly depend on the temperature evolution (this solid simulation gives as results the displacements and the stresses). At the same time, the deformations of the base metal (solid state) due to the temperature gradient can have an effect on the fluid flows (action of solid on fluid), on the morphology of the molten pool, and subsequently, on the temperature field (figure 1). Thus, a physical simulation of the solid/fluid interactions requires the implementation of a strong coupling between the calculations of the fluid flows in the melted pool and stress-strain in the solid.

In this study, a new strategy is proposed to couple, in a physical and pragmatic way, the fluid flows with the solid deformations. It consists in separately calculating the fluid and solid states at each time step using an explicit algorithm. The decoupling of the two states will allow us to avoid the numerical problems related to the strong coupling with an implicit algorithm. The effect of solid deformations on fluid flows (action of solid on fluid) is taken into account by:

- imposing the velocities of solid nodes as boundary conditions at the solid-fluid interface in the thermo-fluid simulation (the thermo-fluid simulation is a simulation coupling fluid flows and heat transfer). These velocities are calculated at each time step by the solid simulation (the solid simulation is based on a purely solid mechanics approach with imposed temperature distributions coming from the thermo-fluid calculation).

- updating the domain occupied by the molten pool which includes the relocation of both the interface between the fluid and solid zones and the fluid-free surface.

This will make it possible to take into account the effect of the solid deformations on the fluid flows and thus on the morphology of molten pool and on the temperature evolution. Note that taking into account the effect of fluid flows and temperature distributions on the calculation of stresses and strains does not require any special attention as it is achieved as usual : the temperature distributions (result of the thermo-fluid simulation) are imposed as loading in the solid computation.

Comparing the proposed strategy with the weak coupling, we note that there is a common point and two points of difference between them. The common point is the decoupling of the solid and fluid states in the problem

equations (the principle of the weak coupling). This allows to avoid the numerical problems related to the use of a strong coupling. The two points of difference are:

- for the solid simulation: with a weak coupling, this simulation is carried out only once at the end of the thermo-fluid simulation. However, our strategy consists in launching a solid simulation after each time step of the thermo-fluid computation.
- for the thermo-fluid simulation: with a weak coupling, the effect of the solid deformations on the fluid flows is neglected whereas it is taken into account with the proposed strategy.

The proposed strategy of coupling therefore allows to simulate, in a physical way, the strong interaction between the solid and the fluid while avoiding the numerical difficulties related to the strong coupling with an implicit algorithm. The steps required to implement this strategy are detailed in section 2.2.2.

Note that some approximations are present in our strategy. In the thermo-fluid simulation, the heat generated in the solid by the plastic dissipation is neglected. In the solid computation, we neglect the influence of the low stresses in the fluid. To summarize, the solid simulation affects the thermo-fluid computation through the solid velocities and the geometry update, and the thermo-fluid computation influences the solid simulation only through the thermal field.

2.2. Implementation of the strategy

The proposed approach has been implemented in the finite element code Sysweld® [33].

2.2.1. Different zones of computation

During the high-temperature process, the material undergoes state changes related to the thermal cycle. This causes transitions from the solid state to the fluid state during heating, and conversely, during cooling. These physical phenomena can be taken into account during the numerical simulation by treating the finite element according to its state. In our approach, three zones are considered:

- the fluid zone: the zone where the material is completely molten.
- the solid zone: the zone where the material is completely solid.

- the mushy zone: the zone where the material is intermediate between liquid and solid. This zone will be treated by the algorithm as a solid zone, but with a particular constitutive law (a different law from that ascribed to the solid zone).

These three zones are separated by two interfaces (figure 2). The first is located between the solid and mushy zones called I_{SM}, and the second between the mushy and fluid zones called I_{MF}. As shown in figure 3, the interfaces between zones coincide with interfaces between finite elements, and never cross elements. Thus, a given finite element always lies entirely within a single zone. One can note that several elements can exist in the mushy zone thickness when the mesh is sufficiently refined.

A transition criterion between these different zones is necessary in order to guide the computation. In our case, the temperature is chosen since it remains a very simple criterion to implement. Just define two temperatures: a solidus temperature T_{sol}, which separates the solid and mushy zones, and a liquidus temperature T_{liq}, which corresponds to the mushy/fluid interface I_{MF}. The average temperature T_{ave} of reference in each finite element will allow it to orient itself towards its computation zone (this average temperature T_{ave} in each finite element is calculated by averaging the temperatures of nodes related to the element). According to this average temperature, the element can be considered as (figure 3):

- a solid element: when its average temperature is less than the solidus temperature ($T_{ave} \leqslant T_{sol}$).
- a mushy element: when its average temperature lies between the solidus and liquidus temperatures ($T_{sol} < T_{ave} < T_{liq}$).
- a fluid element: when its average temperature is larger than the liquidus temperature ($T_{ave} \geqslant T_{liq}$).

We note that different types of node can appear in the mesh (figure 3):

- solid node (red node): it is in the solid zone, in the sense that it is connected to at least one solid element.
- fluid node (green node): it is in the fluid zone, in the sense thatit is connected only to fluid elements.
- fluid/free-surface node (turquoise node): fluid node located on the free surface.
- mushy node (blue node): it is node which is neither "solid" nor "fluid". This node is treated as a solid node during the thermo-fluid simulation.

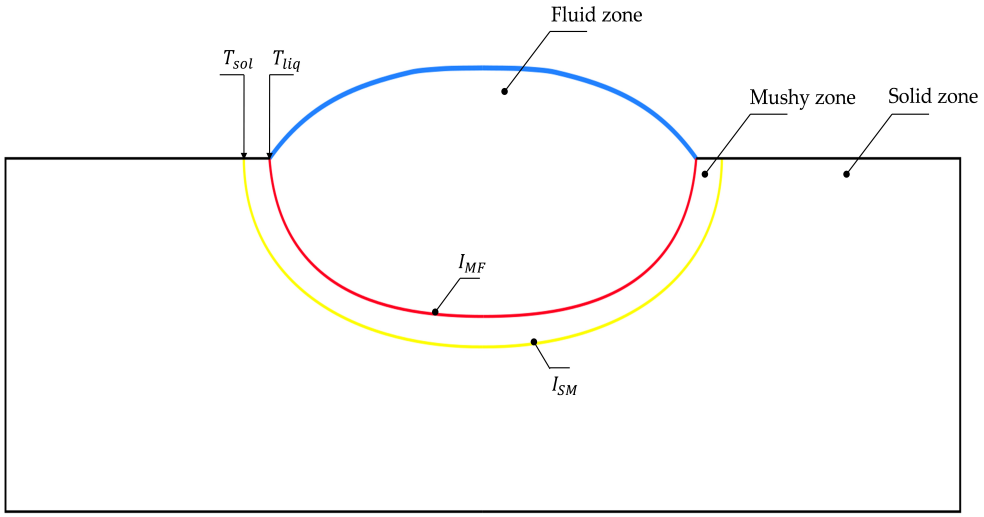

Figure 2: Different computation zones.

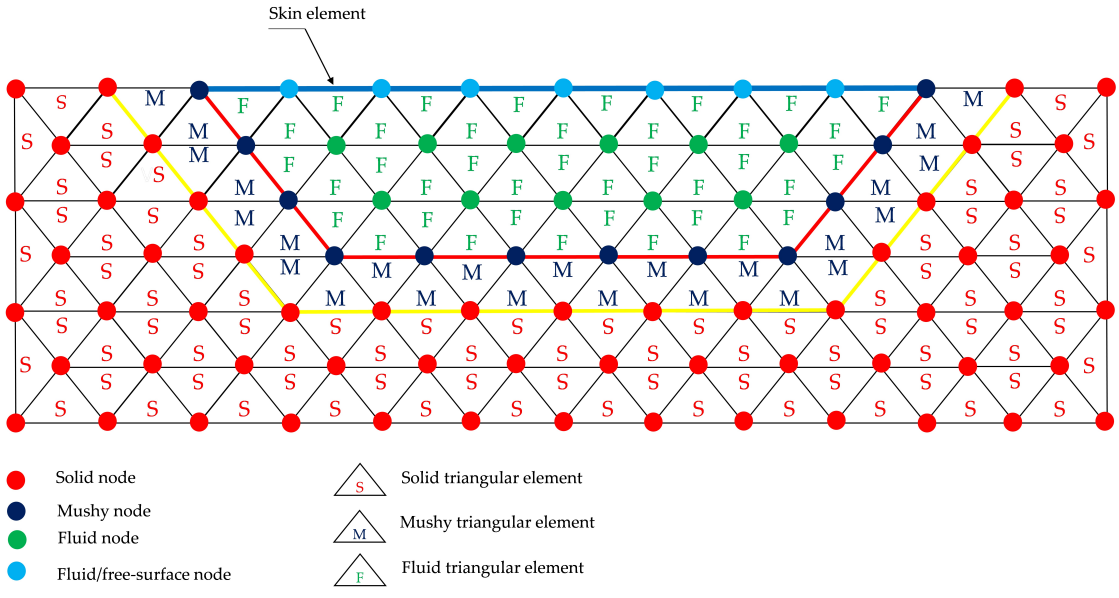

Figure 3: The distinction between the different types of elements and nodes during the thermo-fluid simulation.

2.2.2. Algorithm

In this section, the different steps of the coupling strategy given in figure 4 are detailed. We assume that we are simulating a welding process. Initially, the mesh contains only solid nodes and solid elements. We start with a purely thermal simulation by applying a fixed heat source during an instant t_1 (t_1 can be carried out in several time step: $t_1 = n\Delta t_1$, Δt_1 and n are respectively the time step and the number of time steps during the heating phase), the instant necessary to reach the melting temperature and thus form a molten pool. The temperature field resulting from this first thermal simulation is imposed as loading during the first solid computation at instant t_1 (mechanical simulation with several time steps: $t_1 = n\Delta t_1$). The mesh is then updated based on the displacements resulting from the solid computation. Once the fluid flow are activated (beginning of the thermo-fluid simulation at $t = t_1$ with a new time step Δt), the distinction between the different types of elements and nodes is introduced (figure 3). The fluid flow activation requires the use of small time step compared with that used during the purely thermal simulation ($\Delta t_1 \gg \Delta t$).

Before launching the time step of the solid computation at $t = t_1 + \Delta t$, a mesh update is carried out by moving the fluid and fluid/free-surface nodes (the ALE approach developed by Saadlaoui et al. [21] is used for this updating). We note that, for the moment, the action of the solid onto the fluid is not taken into account (the sole action of the fluid onto the solid is taken into account), but these simulations are necessary to start the loop at $t = t_1 + 2\Delta t$.

Once in the loop, we start to simulate the action of the solid onto the fluid by imposing solid velocities V_s as boundary conditions on the mushy/fluid interface in the thermo-fluid simulation (figure 5). The velocity is continuous throughout the mesh and a no-slip condition is used on the mushy/fluid interface. For the first time step of the loop ($t = t_1 + 2\Delta t$), these solid velocities are calculated from the solid displacements at times $t = t_1$ and $t = t_1 + \Delta t$ (equation 1), hence the necessity to have the results of these two instants before starting the loop:

$$V_s = \frac{U_{t_1+\Delta t} - U_{t_1}}{\Delta t} \tag{1}$$

Imposing these solid velocities will allow to take into account the effect of the solid deformations on the fluid flows and thus, on the morphology of molten pool and on the temperature evolution. The latter is then imposed as loading in the solid simulation at $t = t_1 + 2\Delta t$. The nodes inside the fluid zone and the ones located on the free surface have a nil increment of displacement during the solid simulation. The mechanical behavior of each

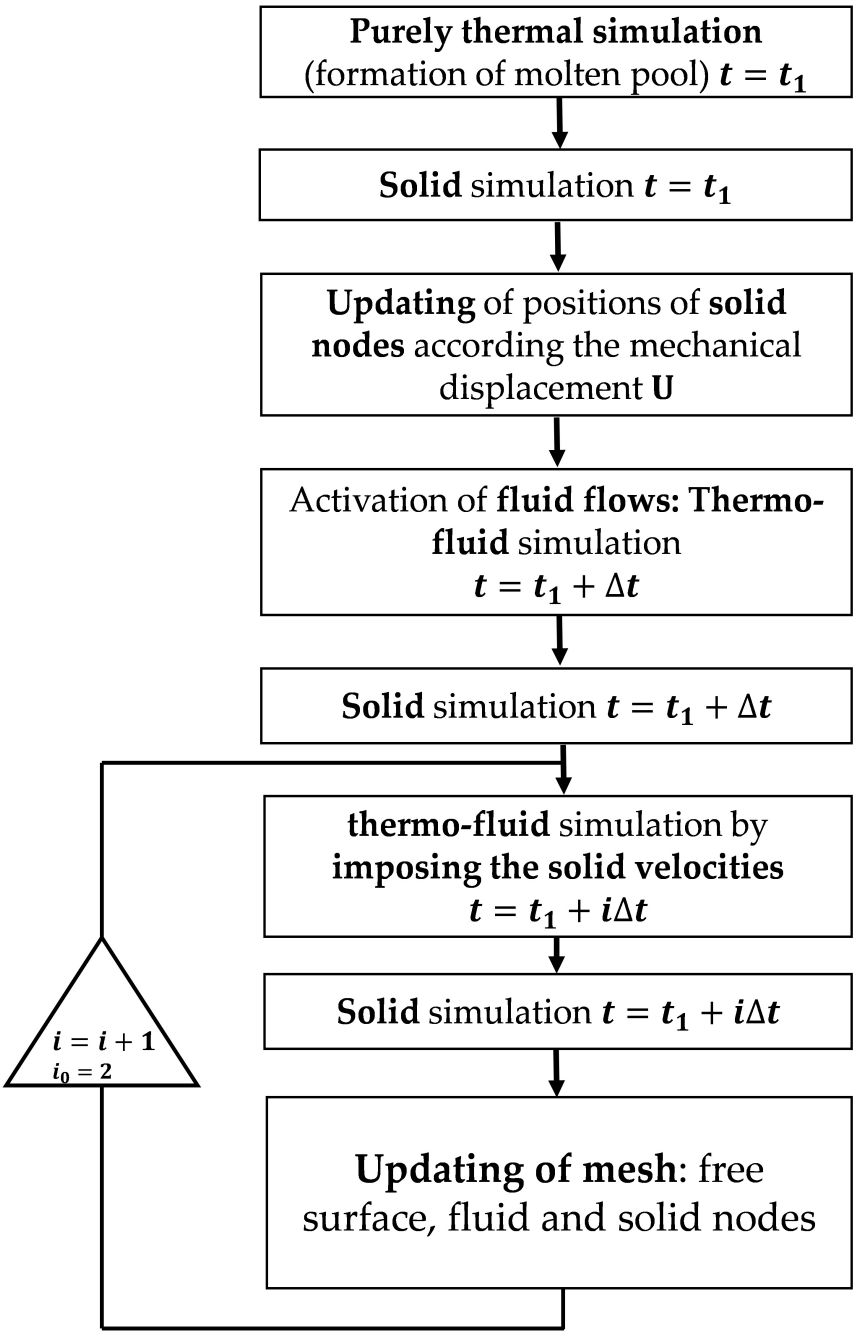

Figure 4: Explicit COUPLING algorithm between fluid and solid states.

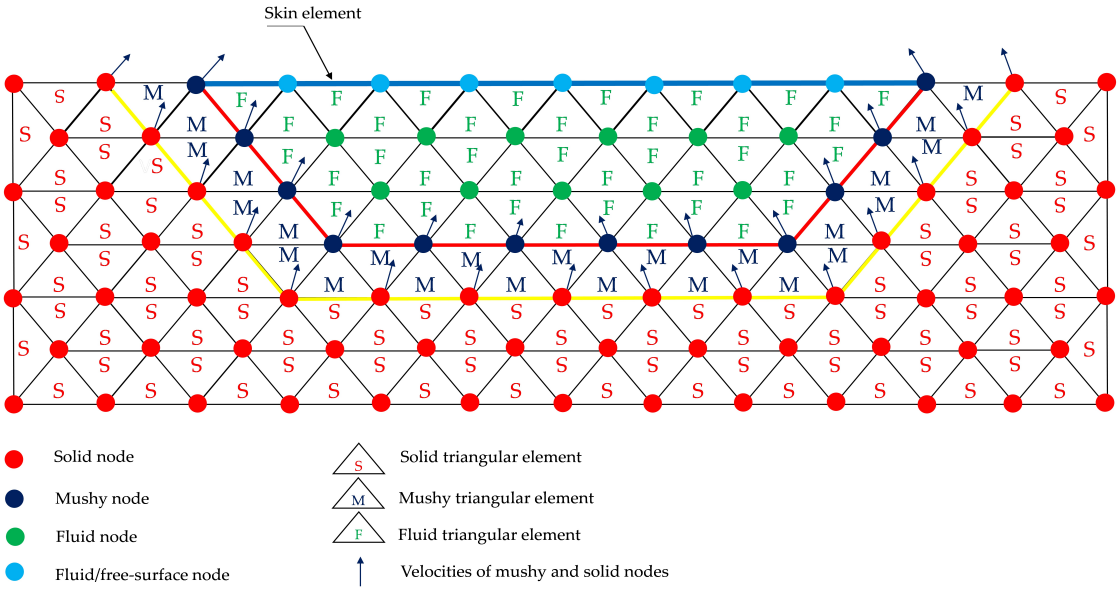

Figure 5: Enforcement of the velocities of solid nodes during the thermo-fluid simulation.

finite element depends on its state (solid, mushy or fluid) during this solid simulation. The mechanical behaviors of these three states are described in section 2.3. The last step of the strategy is to update the mesh by moving the different types of nodes (solid, mushy, and fluid). The approach used to update the mesh is detailed in section 2.2.3. Of course, the simulation in the loop continues until reaching the final instant of computation $t = t_{final}$. Equation 2 is used to calculate the velocity at each solid node all along the loop:

$$V_{s_t} = \frac{U_{t-\Delta t} - U_{t-2\Delta t}}{\Delta t} \tag{2}$$

Here V_{s_t} is the solid velocity of a given node at instant t, $U_{t-\Delta t}$ and $U_{t-2\Delta t}$ are respectively the solid displacements of this node at instants $t - \Delta t$ and $t - 2\Delta t$.

The thermo-fluid and solid computations are carried out on the whole mesh (the same mesh and the computer code Sysweld® are used for these two computations). First, the thermo-fluid computation allows us to calculate heat transfer in the whole structure and fluid flow in the fluid zone (the mushy and solid zones are considered as having a Newtonian fluid behavior with a very high viscosity). Then, the solid computation is carried out to obtain the displacements in the mushy and solid zones, taking into account, as input data, the temperatures given by the thermo-fluid simulation. So,

one can talk about a thermo-mechanical computation since thermal strains are taken into account and computed from the temperature known a priori. During this solid computation, the fluid and fluid/free-surface nodes do not move. Indeed, the displacements of these nodes are computed by the ALE approach, assuming that the fluid zone is a soft solid (very low Young's modulus). To summarize, this means that heat flow in the solid zone is accounted in the thermo-fluid simulation. On the other hand, the stresses in the fluid zone are very low so the presence of this zone has no real effect upon the mechanical fields in the solid zone during the solid simulation.

2.2.3. Updating of the mesh

In this section, we detail the approach of the updating of the node positions of the different zones, namely the solid, the mushy and the fluid zones. The ALE approach developed by Saadlaoui et al. [21] is adapted during this study to update the mesh. Initially, this approach was used by Saadlaoui et al. [21] to follow the evolution of the free surface during a thermo-fluid simulation of laser welding.

Chen at al. [34, 35] have developed a coupling algorithm similar to one proposed here. It allows taking into account the fluid/solid interaction while decoupling the resolution of heat transfer, fluid flow, and solid mechanics. The major difference compared to their work concerns the treatment of the free surface evolution. Indeed, their algorithm is based on the level set method whereas the one developed in this paper used an ALE approach.

Before starting the loop (figure 4), the mesh geometry undergoes two updates. The first is carried out after the first solid simulation ($t = t_1$). Here, the nodes move according to the calculated displacements. The second update is realized after the first time step of the thermo-fluid computation ($t = t_1 + \Delta t$). In this case, the ALE approach developed by Saadlaoui et al. [21] is used. It allows to move the fluid/free-surface nodes and to reposition the internal fluid nodes, while the mushy and solid nodes remain fixed. Once the loop is started, this ALE approach is adapted to take into account the displacements of the different types of nodes. As shown in figure 4, this modified approach updates the mesh after each time step of the thermo-fluid and solid simulations. The displacement of each node is calculated according to its position and state:

- displacement of a mushy or solid node U_s: the calculation of this displacement doesn't need any particular attention since it is directly given by the solid simulation.

- normal displacement of a fluid/free-surface node $\mathbf{U}_{ffs}$ (normal displacement of the free surface): it is calculated as follows using the velocity

of the node coming from the thermo-fluid simulation:

$$\mathbf{U}_{ffs} = (\mathbf{n}.\mathbf{V}_{\mathbf{ffs}})\mathbf{n} \quad \Delta t \tag{3}$$

where $\mathbf{V}_{\mathbf{ffs}}$ is the material velocity of the fluid on the free surface, $\mathbf{n}$ is the outward normal vector to the free surface and Δt is the time step of the thermo-fluid simulation.

- displacements of fluid nodes inside the molten pool (and not at the free surface) U_f: contrary to the displacements of fluid/free-surface nodes, these displacements are totally arbitrary and not physical. Here, the fluid nodes inside the weld pool must in turn be repositioned in order to maintain a good mesh quality. To calculate this displacement, an elastic simulation using a low Young modulus is carried out by imposing as loading the normal displacements of fluid/free-surface nodes (ALE approach: figure 6).

We note that the calculation of these different types of displacements is achieved in the order in which they were cited. As is shown in figure 7, the mesh is then updated according to these displacements.

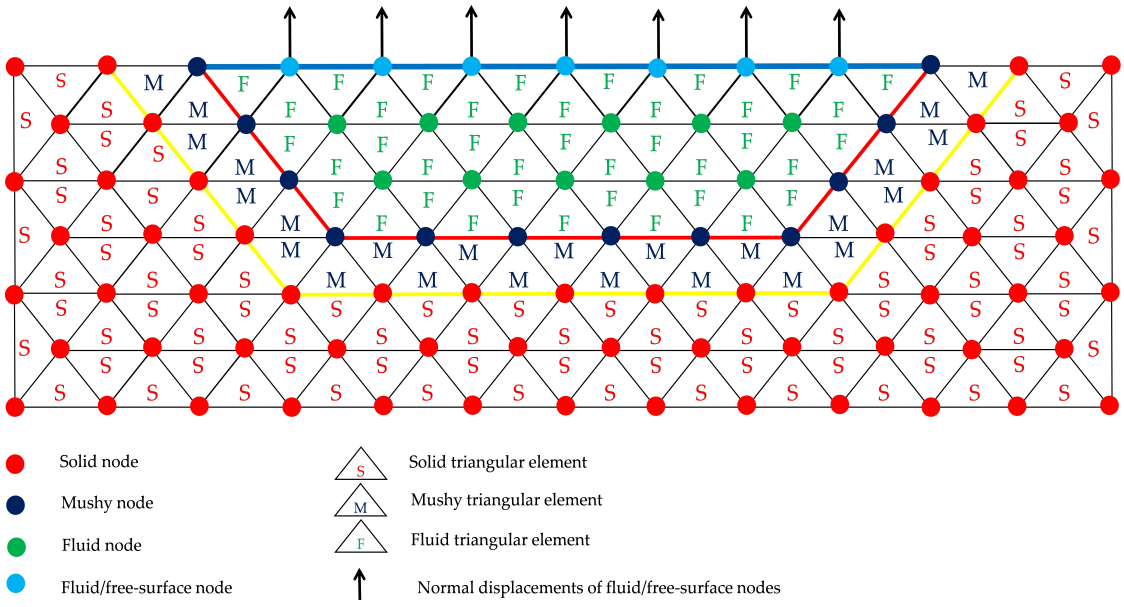

Figure 6: The normal displacements of the fluid/free-surface nodes imposed during the elastic simulation.

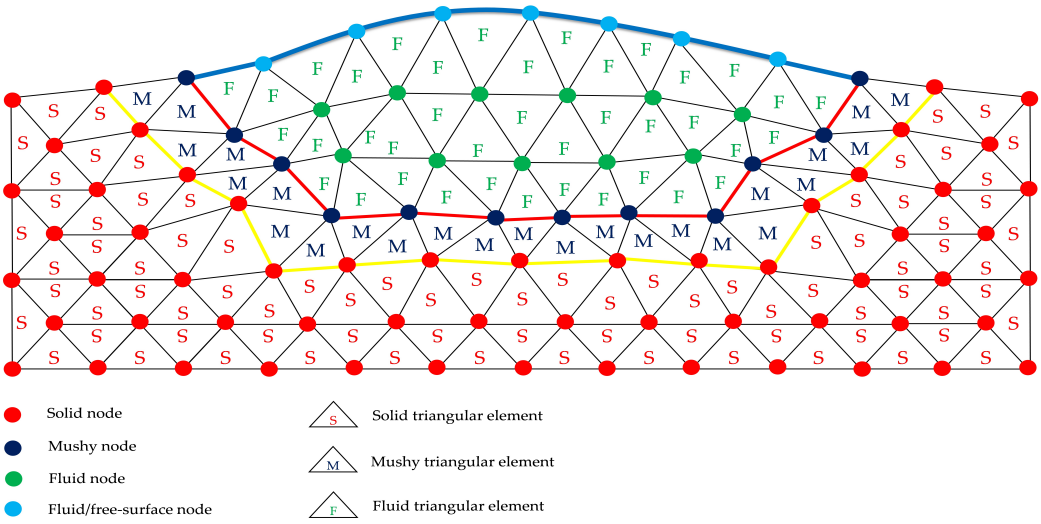

Figure 7: Positions updating of fluid/free-surface, fluid, mushy, and solid nodes.

2.3. Mechanical behavior laws of the different states

During high-temperature processes, the material may be in different states: fluid, mushy or solid (figure 2). The modeling of these different states requires the attribution of specific constitutive laws to each state. In this context, several constitutive laws have been developed to simulate separately the solid and fluid states. Elastoplastic or elastoviscoplastic behaviors and a Newtonian behavior are usually used for solid and fluid simulations respectively [11, 35, 36, 37]. However, the modeling of the mushy zone (a mixture of fluid and solid) is not always obvious. Because of this, the modeling of this zone has often been excluded by the authors [11, 27, 37, 38].

In this study, specific mechanical constitutive laws are assigned to the different states, including the mushy state. Moreover, since our coupling strategy is based on the decoupling of the thermo-fluid and solid simulations, the constitutive law for each state depends on the type of simulation (thermo-fluid or solid) (table 1).

2.3.1. Behavior law of the fluid zone

In the thermo-fluid simulation, the approach developed by Saadlaoui et al. [21] is used and a Newtonian fluid behavior is assigned to the fluid zone.

During the solid computation, the fluid zone is modeled by a Newtonian fluid behavior. Since the fluid nodes do not move during this simulation, the mechanical behavior plays no role in this zone.

Table 1: Constitutive laws of the different states.

States	**Constitutive laws for the thermo-fluid simulation**	**Constitutive laws for the solid simulation**
Fluid	Newtonian fluid	Newtonian fluid
Mushy	Newtonian fluid with a very high viscosity	behavior of fluid-solid mixture
Solid	Newtonian fluid with a very high viscosity	elasto-plastic or elasto-viscoplastic behavior

2.3.2. Behavior law of the solid zone

The solid zone is considered as a fluid with a high viscosity in the thermo-fluid simulation. Here, it is not necessary to assign a constitutive law to the solid since the velocities of all the solid nodes are imposed as loading when the solid/fluid interaction is simulated.

In the solid simulation, any classical elasto-plastic or elasto-viscoplastic constitutive law with isotropic or kinematic hardening can be considered.

2.3.3. Behavior law of the mushy zone

In the thermo-fluid simulation, the mushy zone is considered as a fluid with a high viscosity as in the solid zone.

For the solid simulation, a behavior law must be defined to calculate the stresses in the mushy zone and to ensure the transition between fluid and solid behaviors. Such laws have been proposed by different authors for casting or welding simulations [39, 40, 41, 42]. The modeling used [42] assumes the coexistence of solid and fluid phases in the temperature range of the mushy zone ($T_{sol} < T_{mushy} < T_{liq}$). As is shown by the rheological diagram (figure 8), this law is based on a mixed parallel-serie behavior. The parallel model deals with the deviatoric part of the stress tensor and the serie model deals with the spherical part. The pressure and the strain deviator are supposed to be the same in both states. Both states are supposed to have the same bulk modulus (the mean strain is also supposed the same in both states). The indexes S and F, denoting the solid and fluid states, state of the stress in the mixture that is given by:

$$\sigma = s + pI \tag{4}$$

with,

$$s = f_F s_F + f_S s_S \tag{5}$$

$$p = p_F = p_S \tag{6}$$

where σ, s and $p = \frac{1}{3}tr(\sigma)$ are respectively the stress tensor, its deviator and the hydrostatic pressure. f_S and f_F are the solid and fluid fractions respectively; they depend only on temperature with $f_S + f_F = 1$. T_{liq} and T_{sol} being the liquidus and solidus temperatures respectively, the fluid fraction f_F is calculated from the temperature T of the material as follows:

$$\left\{ \begin{array}{lcl} f_F & = & 1 \quad if \quad T \geq T_{liq} \\ f_F & = & \frac{T - T_{sol}}{T_{liq} - T_{sol}} \quad if \, T_{sol} \leq T \leq T_{liq} \\ f_F & = & 0 \quad if \quad T \leq T_{sol} \end{array} \right. \tag{7}$$

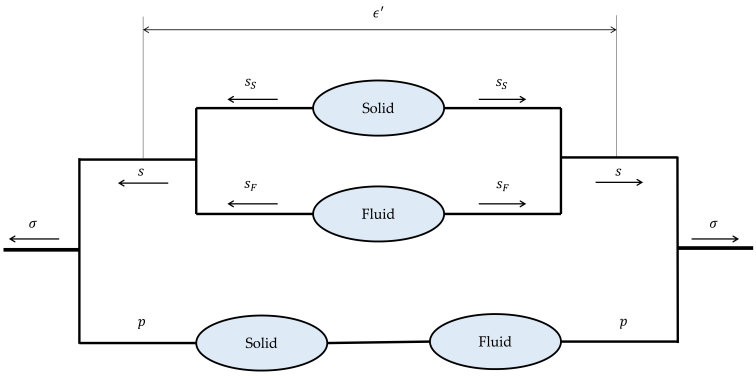

Figure 8: Rheological scheme of mixed behavior.

The pressure in the mixture is calculated from the mean strain and the common bulk coefficient of the two phases. The deviatoric part of the stresses in the fluid and solid phases is calculated according to their constitutive laws. The liquid phase is supposed to obey a Newtonian fluid behavior. The stress deviator is related to the strain rate deviator as follows :

$$s_F = 2\mu_F.\dot{\epsilon}' \tag{8}$$

where μ_F is the viscosity of the fluid.

Any kind of elasto-plastic or viscoplastic constitutive law may be used for the solid phase. If a fluid→solid transformation occurs between t and $t + \Delta t$, the equation of evolution of the hardening internal variables of the solid phase must then account for:

- the hardening of the solid phase fraction pre-existing at instant t

- the fluid fraction that becomes solid between t and $t + \Delta t$ and which starts its solid history with internal variables equal to zero (no hardening inherited from the fluid past).

Details concerning these equations of evolution in the case of phase transformations can be found in [43].

2.3.4. Finite element formulation

The thermo-fluid and solid simulations are achieved using the same tetraedral mesh, thus avoiding any transfer of the displacement or velocity fields between both problems. But different finite element formulations are used.

For the thermo-fluid simulation, the element P1+/P1 is used [44]. This element rests upon a mixed velocity-pressure formulation and can deal with fully incompressible problems. A first order the approximation is considered for the pressure and for the velocity field, the approximation in enriched using additional internal degrees of freedom associated with a bubble function [21].

For the solid simulation, the P1/P1 element developed by Feulvarch et al. [45] is used as it has exhibited a more efficient behavior than the P1+/P1 element as far as elasto-plastic or viscoplastic problems are concerned. This element also rests upon a mixed displacement-pressure formulation with first order approximations for both the displacement and pressure fields. The mixed formulation is stabilized by using an incremental formulation including an anisotropic diffusion term as proposed by Feulvarch et al. [45, 46].

3. Numerical simulation of the solid/fluid interaction: laser welding

3.1. FE model

In this section, a 3D thermo-fluid-mechanical simulation of laser welding by conduction (without keyhole formation) is presented. It takes into account the fluid flows through the two effects of the surface tension and the buoyancy. A metal block with $20\,mm$ length, $10\,mm$ width and $3\,mm$ height is simulated. Only half of the structure is modeled because of symmetry reasons. The mesh given by figure 9 includes $179,544$ tetrahedral elements, $10,550$ triangular elements (skin elements used to apply the two effects of the surface tension [29]), and $34,983$ nodes. In the fluid zone, the element size is equal to $300\,\mu m$, and it can reach $2000\,\mu m$ in the solid zone. The stainless steel grade 316L is used. All the data pertaining to this material are given by figures 10 and 11 [47, 48]. As shown in these figures, the material properties depend on the temperature. As far as the thermo-fluid computation is concerned, the variation of density according to the temperature (buoyancy forces) allows us taking into account of the thermal dilatation in the

different zones (fluid, mushy, and solid zones). During the solid simulation, the variation of the thermal expansion coefficient allows us to consider the thermal dilatation in the mushy and solid zones. This dilatation is not taken into account in the fluid zone since the fluid nodes are fixed.

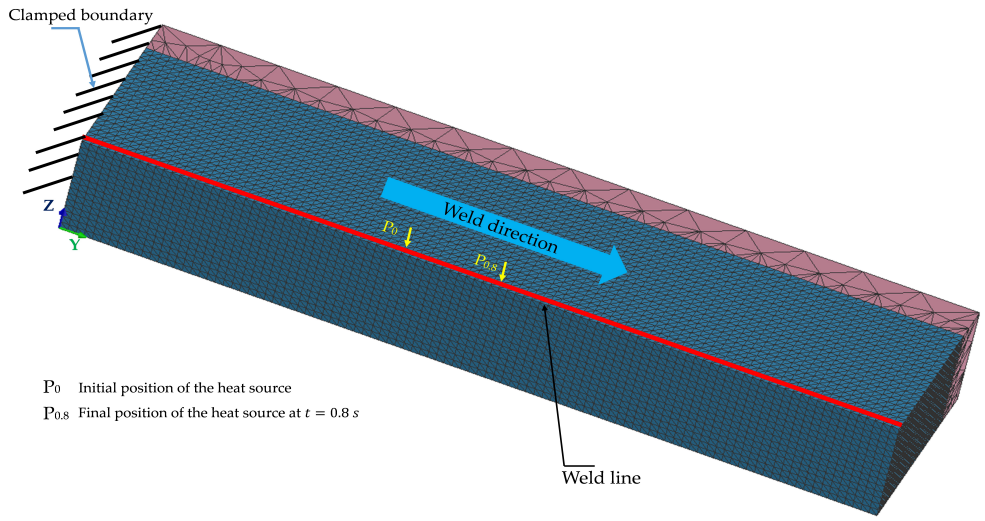

Figure 9: Mesh.

An equivalent double ellipsoidal heat source (figure 12) [49] is applied in the welding direction to achieve a single-pass laser with a welding speed equal to $v_{welding} = 6\,mm.s^{-1}$. Laser power density of $1000\,MW.m^{-3}$ is applied (with a maximal front source intensity of 55 and a maximal rear source intensity of 45). It is assumed that $100\,\%$ of the laser power is absorbed. A front length "f" of $2.5\,mm$, rear length "r" of $4.33\,mm$, half-width "h" of $3\,mm$, and penetration "p" of $2\,mm$ are used to define the heat source dimensions (figure 12). The heating time is $0.8\,s$, including $0.4\,s$ for the creation of the molten pool (thermal computation with static heat source and without fluid flows), and $0.4\,s$ for the thermo-fluid simulation (with fluid flows) with the motion of heat source. The part is then cooled until the end of the simulation at $t_{end} = 1.5\,s$. The time step is equal to $0.1\,s$ for the creation of the molten pool and $2.5\,.\,10^{-4}\,s$ after the activation of the fluid flows.

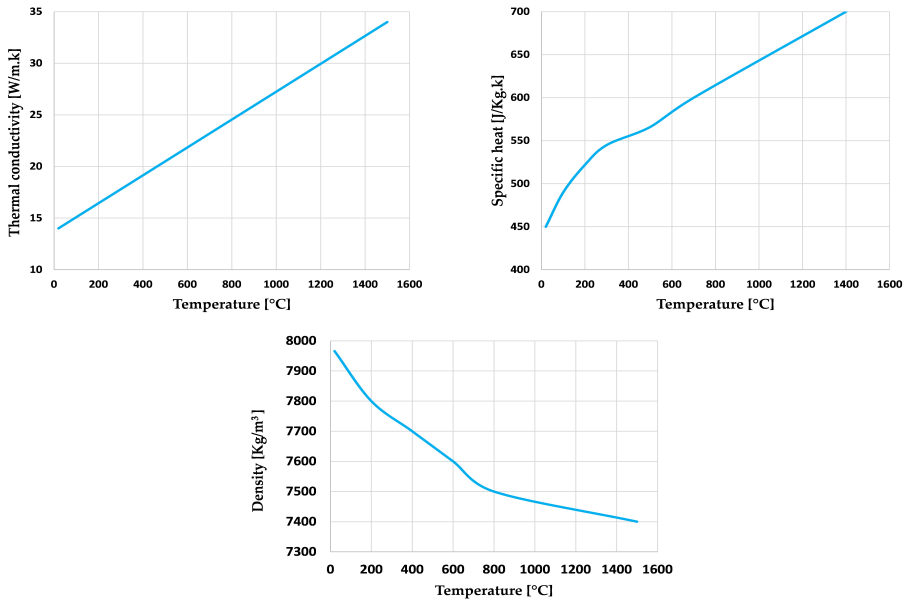

Figure 10: Thermo-physical proprities of the stainless steel: 316L.

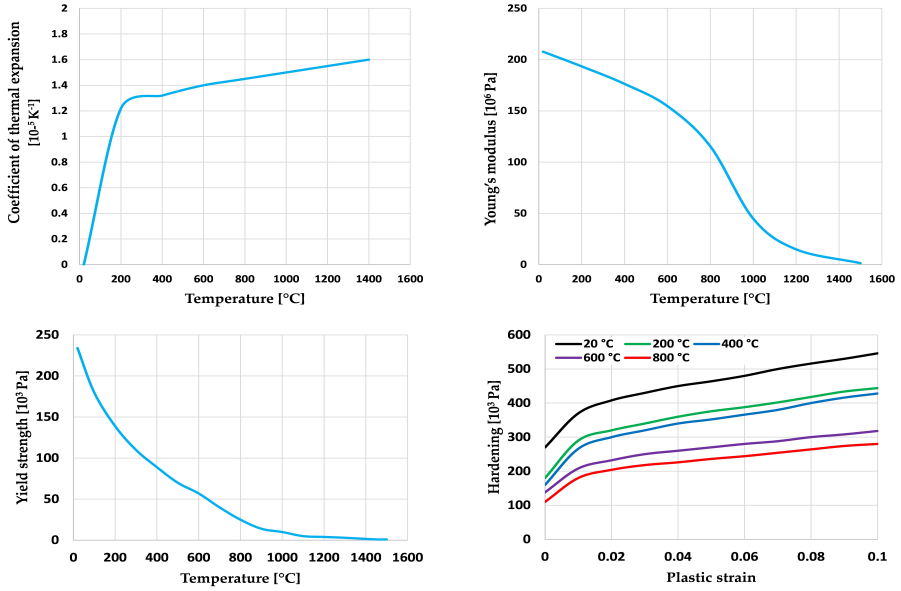

Figure 11: Mechanical proprities of the stainless steel: 316L.

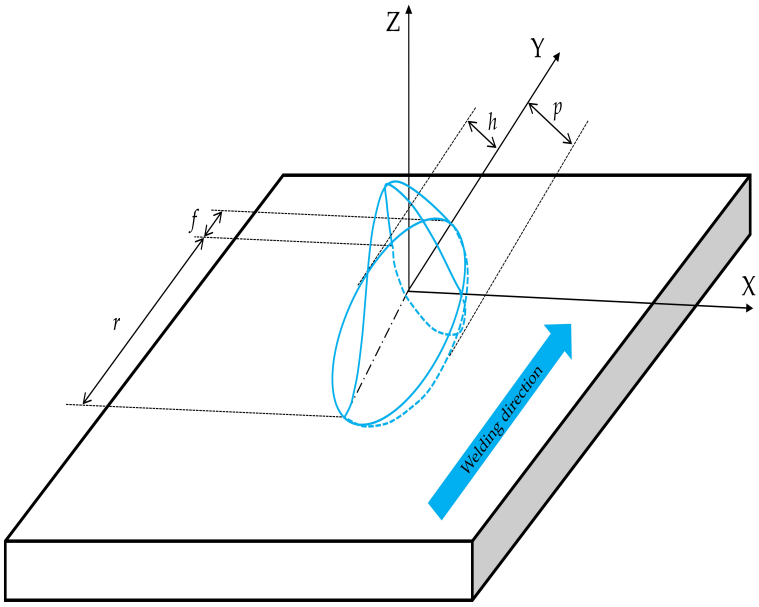

Figure 12: Schematic view of the heat source used.

Heat exchanges due to convection and radiation on the boundary with the external medium are taken into account:

$$\phi = \phi_{convection} + \phi_{radiation} \tag{9}$$

with

$$\phi_{convection} = h(T - T_0) \tag{10}$$

$$\phi_{radiation} = \epsilon\,\sigma_0(T^4 - T_0^4) \tag{11}$$

where $h = 40\,W.m^{-2}.K^{-1}$ is the transfer coefficient, $T_0 = 293\,K$ the room temperature, $\sigma_0 = 5.67^{-8}\,W.m^{-2}.K^{-4}$ the Stefan-Boltzmann constant, and $\epsilon = 0.7$ is the emissivity. These conditions are enforced on all mesh faces except the symmetry plane, where an insulating condition is imposed.

During the thermo-fluid simulation, in the mushy and solid zones, the elements are assumed to have a high dynamic viscosity $\mu = 10^6\,Kg.m^{-1}.s^{-1}$. In the fluid zone, the elements have a dynamic viscosity equal to $\mu_F = 6.2\,10^{-2}\,Kg.m^{-1}.s^{-1}$. A temperature-dependent surface tension $\gamma = \gamma_L + \alpha(T - T_L)$ with $\gamma_L = 0.45\,N.m^{-1}$, $T_L = 1500\,°C$, and $\alpha = 2.10^{-4}\,N.m^{-1}.K^{-1}$ is taken into account to include both the "curvature" and "Marangoni" effects.

For the solid simulation (mechanical simulation), an elasto-plastic behavior with isotropic hardening is used. The mechanical properties (Young modulus, yield strength, and hardening) are temperature dependent (figure

11).
The mechanical boundary conditions are:

- $U_x = 0$ on the symmetry plane.
- Clamped boundary on the left side (figure 9).

To study the effect of the solid/fluid coupling on thermo-fluid results (flow velocity and morphology of the molten pool), two simulations are carried out:

- Thermo-fluid-mechanical simulation "A" using a weak coupling (standard version of Sysweld®): it consists in taking into account the fluid flows, but neglecting the effect of solid deformations on fluid flows.
- Thermo-fluid-mechanical simulation "B" using our coupling strategy (our new version implemented in Sysweld®): during this simulation the fluid flows and the effect of solid deformations on fluid flows are taken into account.

3.2. Results and discussion

The thermo-fluid-mechanical simulation based on the coupling strategy developed (case B) can give as results the temperature field and fluid flows during the laser welding process. Figures 13 and 14 show respectively the distributions of the temperature and fluid velocity at two instants ($t = 0.5$ and $t = 0.6\,s$) on the deformed mesh under the effect of the free surface. This simulation can also give as results the mechanical fields. For example, the figure 15 shows the average strain at two instants ($t = 0.5$ and $t = 0.6\,s$). In this study, we will focus on the results of the solid/fluid interaction.

In this section, a comparison of the results of the weak coupling and our coupling strategy are given. Figure 16 shows the distribution of the fluid velocity for the two types of coupling strategy ("A" and "B"). It can summarize the difference between these two strategies "A" and "B". The first difference is the effect of the solid deformations on the fluid flows. This effect is considered during the "B" simulation by imposing solid velocities at each time step of the thermo-fluid simulation. For this reason, we find fluid velocities outside the fluid zone (the imposed solid velocities) during the "B" simulation (figure 16). These solid velocities are the order of $0.002\,m.s^{-1}$. During the "A" simulation, the solid/fluid interaction (effects of the solid deformations on fluid flows) is neglected. Thus, the flow velocities exist only in the fluid zone. They are induced by the fluid flow in the molten pool (maximal velocities of the order of $0.2\,m.s^{-1}$). The second point of difference is the update of the mesh, taking into account the displacements of the solid

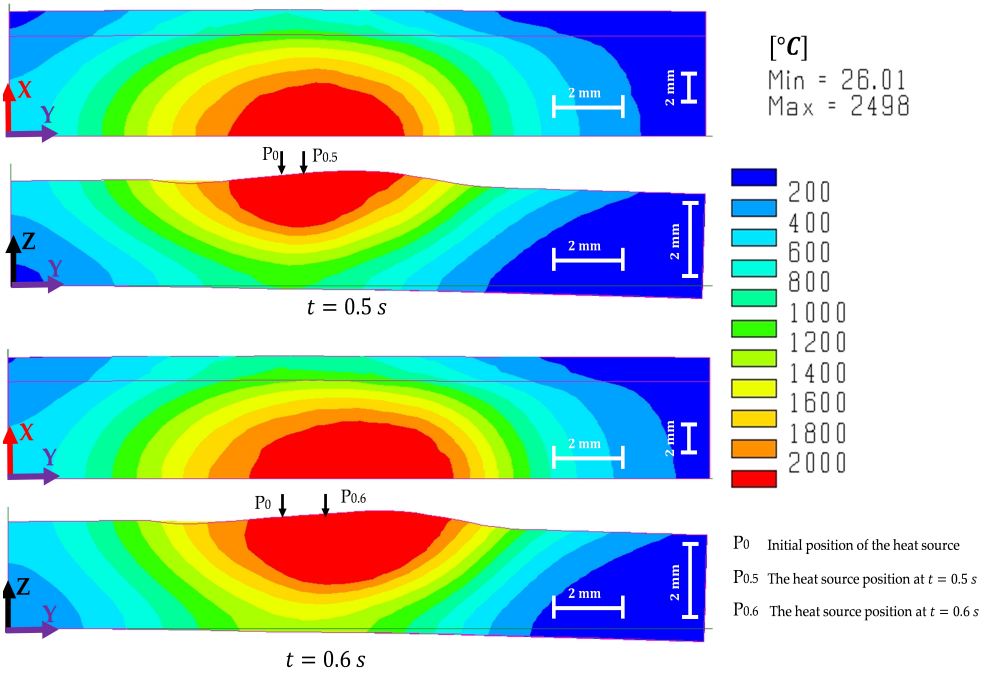

Figure 13: Distributions of the temperature at $t = 0.5s$ and $t = 0.6s$ on the deformed mesh (case B).

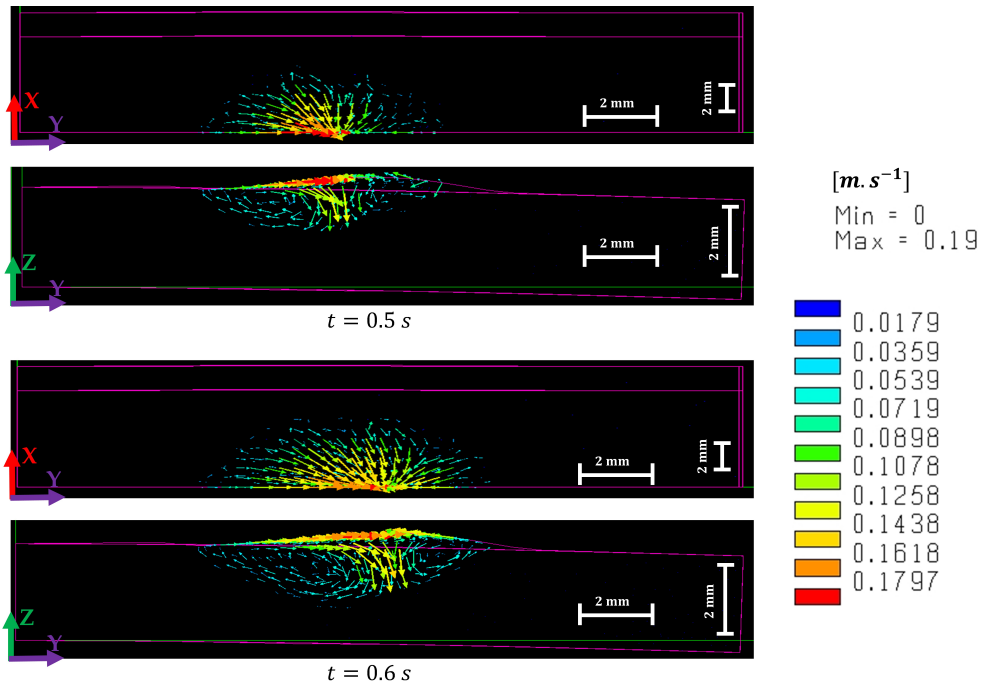

Figure 14: Distributions of the fluid velocity at $t = 0.5s$ and $t = 0.6s$ on the deformed mesh (case B).

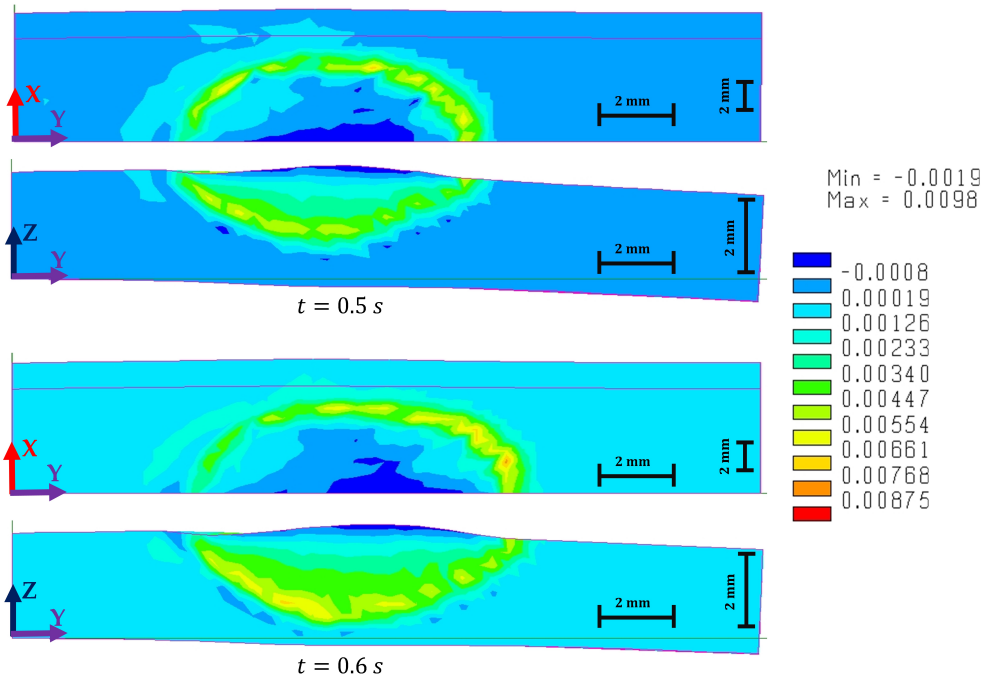

Figure 15: Distributions of the average strain at $t = 0.5s$ and $t = 0.6s$ on the deformed mesh (case B).

nodes U_s (vertical deflection of the block). As shown in figure 16, the "B" strategy allows the mesh to be updated by using the displacements of the fluid nodes (including the free surface nodes) and the solid nodes (including the mushy nodes). In the "A" case, only the displacements of the fluid nodes (including the free surface nodes) are taken into account for the update of the mesh.

A comparison of the results (fluid velocity and displacement of the free surface) in the weak coupling and our coupling strategy are given by figures 17 and 18. Figure 17 shows the evolution of the fluid velocity at different instants during the two simulations ("A" and "B"). We note that the solid deformations (the imposed solid velocities) has a minor effect on the flow velocities in the weld pool. The flow velocities of the "B" simulation (using our coupling strategy) are lower than those of the "A" simulation. A maximum gap of about 28 % is found.

The evolution of the free surface at different instants during these two simulations is given by figure 18. We note a minor effect of the solid deformations on the free surface and thus on the morphology of the weld pool. A maximal gap of 15 % is found between the displacements of the free surface of the two simulations ("A" and "B"). This minor effect can be explained by

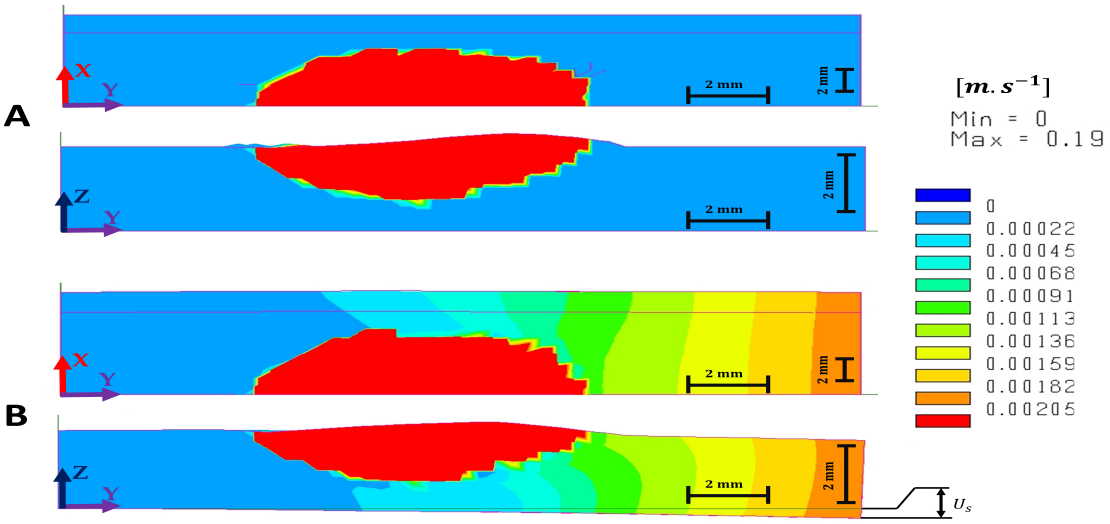

Figure 16: Magnitude of the velocity for both simulations (A and B) at $t = 0.6s$.

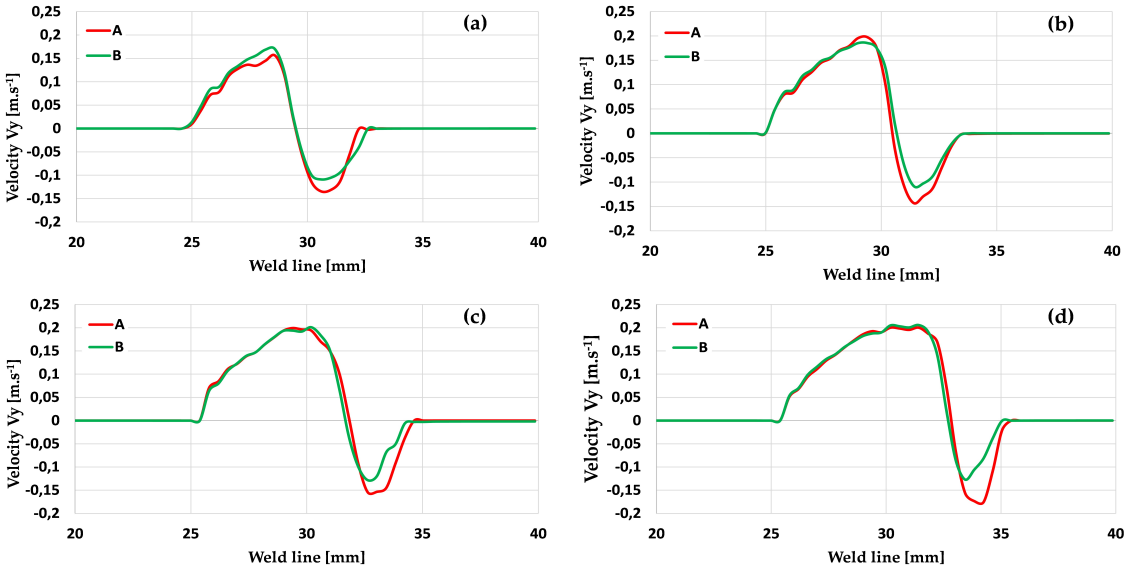

Figure 17: Solid/fluid effect on the flow velocity in the molten pool along the weld line: (a) $t = 0.5s$; (b) $t = 0.6s$; (c) $t = 0.7s$; (d) $t = 0.8s$.

the fact that the displacement of the free surface is calculated from the flow velocities of this surface. These velocities are little sensitive to the solid/fluid coupling (figure 17).

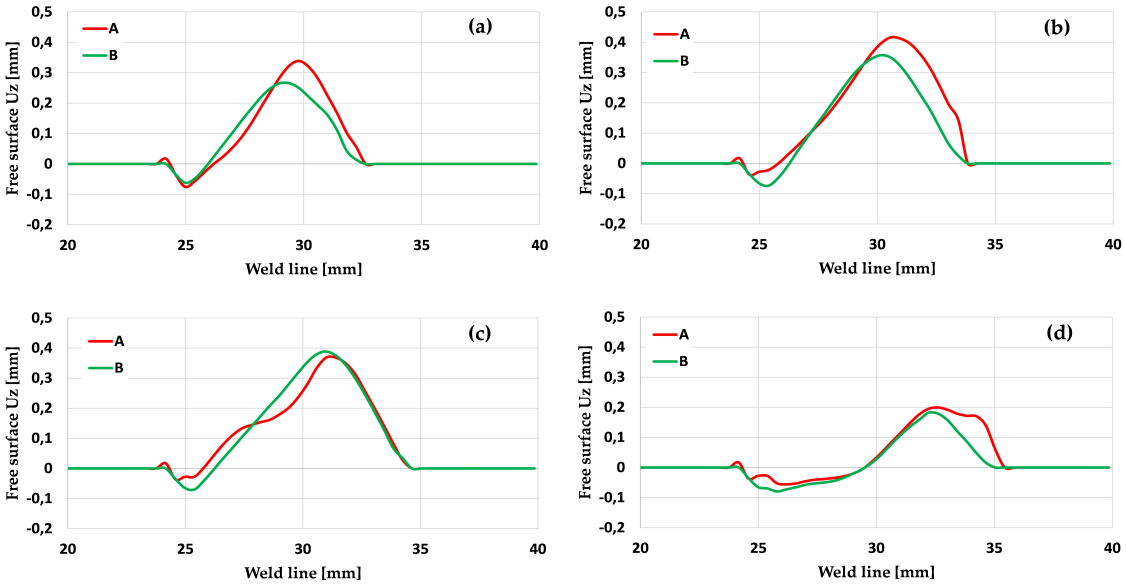

Figure 18: Solid/fluid effect on the free surface along the weld line: (a) $t = 0.5s$; (b) $t = 0.6s$; (c) $t = 0.7s$; (d) $t = 0.8s$.

This study shows that the solid/fluid interaction (effect of solid deformations on fluid flows) does not have a great effect on the thermo-fluid results (fluid flows and molten pool morphology) in the example considered. Indeed, during a laser welding process the mechanical displacements (solid displacements) remain very low (in the order of $2.10^{-4}\,m$). So, the solid/fluid interaction can be neglected during the simulation of this process. However, depending on the welding process and the clamping conditions, it may or may not be necessary to include this interaction during the numerical simulation. For example, this interaction needs to be simulated during other processes where the effect of solid deformations on fluid flows are expected to be much higher (spot welding, narrow gap welding, etc.). We also note that accounting for the effects of the fluid flows on the solid deformations are essential during the simulation of thermo-mechanical processes.

4. Conclusion

In order to study the interaction between the fluid flows and the solid deformations during the numerical simulation of thermo-mechanical processes, a new strategy of solid/fluid coupling (strong coupling with an explicit algorithm) was developed. It allows to take into account in a simple and efficient way the effect of the solid deformations in the base metal on the fluid flows in the molten pool. This effect is implemented by imposing solid velocities as loading at each time step of the thermo-fluid simulation and by updating the domain occupied by the molten pool. These solid velocities come at each time step from a solid calculation.

The formulation of the fluid problem developed by Saadlaoui et al. [21] is used to simulate the fluid flows in the molten pool. It allows to take into account the surface tension (including both the "curvature effect" and the "Marangoni effect"), buoyancy forces, and the free surface motion. The ALE approach is adapted to take into account the displacements of free surface nodes, of fluid nodes inside the molten pool and of solid nodes in the base metal.

A 3D thermo-fluid-mechanical simulation of laser welding by conduction was carried out. It gives qualitatively acceptable results in terms of the velocity field and the evolution of the free surface [32, 50]. To study the effect of the solid deformations in the base metal on the fluid flows in the weld pool, a comparison of the results of two simulations was performed. The first simulation used a weak coupling, neglecting the solid/fluid interaction (effects of the solid deformations on fluid flow). Our coupling strategy was used in a second simulation. The comparison has shown that the solid deformations do not have a big effect on the flow velocity, free surface evolution and molten weld morphology. Indeed, during a laser welding process the mechanical displacements (tied to the solid deformations) remain very low (of the order of $2.10^{-4}\,m$). The solid/fluid interaction can therefore be neglected for the simulation of this process. However, the effect of the solid deformations on the fluid flows in the molten pool depends on the welding process and clamping conditions. For example, this effect should be much larger in the case of narrow gap welding or for resistance spot welding, that are the subject of work in progress.

Acknowledgements

The authors would like to thank ESI-GROUP for funding this study.

References

[1] P. Duranton, J. Devaux, V. Robin, P. Gilles, and J. M. Bergheau. 3D modelling of multipass welding of a 316L stainless steel pipe. *Journal of Materials Processing Technology*, 153-154:457–463, November 2004.

[2] P. Martinson, S. Daneshpour, M. Koçak, S. Riekehr, and P. Staron. Residual stress analysis of laser spot welding of steel sheets. *Materials & Design*, 30(9):3351–3359, October 2009.

[3] M. Medale, S. Rabier, and C. Xhaard. A Thermo-Hydraulic Numerical Model for High Energy Welding Processes. *Revue Européenne des Éléments Finis*, 13(3-4):207–229, January 2004.

[4] M. Medale, C. Touvrey, and R. Fabbro. An axi-symmetric thermo-hydraulic model to better understand spot laser welding. *European Journal of Computational Mechanics*, 17(5-7):795–806, January 2008.

[5] T.D. Anderson, J.N. DuPont, and T. DebRoy. Origin of stray grain formation in single-crystal superalloy weld pools from heat transfer and fluid flow modeling. *Acta Materialia*, 58(4):1441–1454, February 2010.

[6] M. Bellet and M. Hamide. Direct modeling of material deposit and identification of energy transfer in gas metal arc welding. *International Journal of Numerical Methods for Heat & Fluid Flow*, 23(8):1340–1355, October 2013.

[7] O. Desmaison, M. Bellet, and G. Guillemot. A level set approach for the simulation of the multipass hybrid laser/GMA welding process. *Computational Materials Science*, 91:240–250, August 2014.

[8] M.C. Nguyen, M. Medale, O. Asserin, S. Gounand, and P. Gilles. Sensitivity to welding positions and parameters in GTA welding with a 3D multiphysics numerical model. *Numerical Heat Transfer, Part A: Applications*, 71(3):233–249, February 2017.

[9] H.L. Wei, J.W. Elmer, and T. DebRoy. Crystal growth during keyhole mode laser welding. *Acta Materialia*, 133:10–20, July 2017.

[10] H.L. Wei, J.W. Elmer, and T. DebRoy. Three-dimensional modeling of grain structure evolution during welding of an aluminum alloy. *Acta Materialia*, 126:413–425, March 2017.

[11] E. Feulvarch, V. Robin, and J.M. Bergheau. Thermometallurgical and mechanical modelling of welding – application to multipass dissimilar metal girth welds. *Science and Technology of Welding and Joining*, 16(3):221–231, April 2011.

[12] A. Anca, A. Cardona, J. Risso, and V.D. Fachinotti. Finite element modeling of welding processes. *Applied Mathematical Modelling*, 35(2):688–707, February 2011.

[13] L. Portelette, J.C. Roux, V. Robin, and E. Feulvarch. A Gaussian surrogate model for residual stresses induced by orbital multi-pass TIG welding. *Computers & Structures*, 183:27–37, April 2017.

[14] S. Tsirkas, P. Papanikos, K. Pericleous, N. Strusevich, F. Boitout, and J.M. Bergheau. Evaluation of distortions in laser welded shipbuilding parts using local-global finite element approach. *Science and Technology of Welding and Joining*, 8(2):79–88, April 2003.

[15] P. Lacki and K. Adamus. Numerical simulation of the electron beam welding process. *Computers & Structures*, 89(11-12):977–985, June 2011.

[16] W. Piekarska and M. Kubiak. Modeling of thermal phenomena in single laser beam and laser-arc hybrid welding processes using projection method. *Applied Mathematical Modelling*, 37(4):2051–2062, February 2013.

[17] Z. Zhang, P. Ge, and G.Z. Zhao. Numerical studies of post weld heat treatment on residual stresses in welded impeller. *International Journal of Pressure Vessels and Piping*, 153:1–14, June 2017.

[18] J.D. Caprace, G. Fu, J.F. Carrara, H. Remes, and S.B. Shin. A benchmark study of uncertainness in welding simulation. *Marine Structures*, 56:69–84, November 2017.

[19] S.H. Ko, C.D. Yoo, D.F. Farson, and S.K. Choi. Mathematical modeling of the dynamic behavior of gas tungsten arc weld pools. *Metallurgical and Materials Transactions B*, 31(6):1465–1473, December 2000.

[20] A. Berthier, P. Paillard, M. Carin, F. Valensi, and S. Pellerin. TIG and A-TIG welding experimental investigations and comparison to simulation : Part 1 : Identification of Marangoni effect. *Science and technology of welding and joining*, pages 609–615, 2012.

[21] Y. Saadlaoui, E. Feulvarch, A. Delache, J.B. Leblond, and J.M. Bergheau. A new strategy for the numerical modeling of a weld pool. *Comptes Rendus Mécanique*, 346(11):999–1017, November 2018.

[22] M. Hamide. *Modélisation numérique du soudage à l'arc des aciers*. PhD thesis, Mines ParisTech, 2008.

[23] Y. Saadlaoui. *Simulation numérique des procédés thermomécaniques dans une approche couplant les écoulements du fluide avec les déformations du solide : application au soudage laser et à la fusion d'un lit de poudre*. PhD thesis, Lyon University, Saint Etienne, 2019.

[24] G. Mi, L. Xiong, C. Wang, X. Hu, and Y. Wei. A thermal-metallurgical-mechanical model for laser welding Q235 steel. *Journal of Materials Processing Technology*, 238:39–48, December 2016.

[25] J. Cheon and S.J. Na. Prediction of welding residual stress with real-time phase transformation by CFD thermal analysis. *International Journal of Mechanical Sciences*, 131-132:37–51, October 2017.

[26] J. Xu, C. Chen, T. Lei, W. Wang, and Y. Rong. Inhomogeneous thermal-mechanical analysis of 316L butt joint in laser welding. *Optics & Laser Technology*, 115:71–80, July 2019.

[27] T. Heuzé, J.B. Leblond, and J.M. Bergheau. Modélisation des couplages fluide/solide dans les procédés d'assemblage à haute température. *Mécanique & Industries*, 12(3):183–191, 2011.

[28] H. Amin-El-Sayed. *Simulation numérique du soudage : Couplage des écoulements dans le bain fondu avec les déformations de la partie solide*. PhD thesis, Lyon University, Saint Etienne, 2014.

[29] J.B. Leblond, H. Amin-El-Sayed, and J.M. Bergheau. On the incorporation of surface tension in finite-element calculations. *Comptes Rendus Mécanique*, 341(11-12):770–775, November 2013.

[30] B. Ramaswamy. Numerical simulation of unsteady viscous free-surface flow. *Journal of Computational Physics*, 87(2):495, April 1990.

[31] S. Rabier and M. Medale. Computation of free surface flows with a projection FEM in a moving mesh framework. *Computer Methods in Applied Mechanics and Engineering*, 192(41-42):4703–4721, October 2003.

[32] Z. Zhang and C. Wu. Effect of fluid flow in the weld pool on the numerical simulation accuracy of the thermal field in hybrid welding. *Journal of Manufacturing Processes*, 20:215–223, October 2015.

[33] ESI-GROUP. Reference Analysis Manual, 2015.

[34] Q. Chen, G. Guillemot, C. Gandin, and M. Bellet. Three-dimensional finite element thermomechanical modeling of additive manufacturing by selective laser melting for ceramic materials. *Additive Manufacturing*, 16:124–137, August 2017.

[35] Q. Chen. *Thermomechanical numerical modelling of additive manufacturing by selective laser melting of powder bed: Application to ceramic materials*. PhD thesis, Mines ParisTech, 2018.

[36] E. Feulvarch, J.M. Bergheau, and J.B. Leblond. An implicit finite element algorithm for the simulation of diffusion with phase changes in solids. *International Journal for Numerical Methods in Engineering*, 78(12):1492–1512, June 2009.

[37] M. Dal and R. Fabbro. An overview of the state of art in laser welding simulation. *Optics & Laser Technology*, 78:2–14, April 2016.

[38] H.L. Wei, J.W. Elmer, and T. DebRoy. Crystal growth during keyhole mode laser welding. *Acta Materialia*, 133:10–20, July 2017.

[39] M. Bellet, O. Jaouen, and I. Poitrault. An ALE-FEM approach to the thermomechanics of solidification processes with application to the prediction of pipe shrinkage. *Int Jnl of Num Meth for HFF*, 15(2):120–142, March 2005.

[40] R. Forestier, F. Costes, O. Jaouen, and M. Bellet. Finite element thermomechanical simulation of steel continuous casting. In *Proceedings from the 12th International Conference on Modeling of Casting, Welding, and Advanced Solidification Processes*, pages 295–302, Warrendale-USA, 2009.

[41] I. Tatsuo. *Welding and Casting: Application of Metallo-thermomechanics Part I: Fundamental Framework of the Governing Equations and Simulated Results of Welding Process*. Encyclopedia of thermal stresses, Richard B. Hetnarski editor, 2014.

[42] H. Sallem, E. Feulvarch, H. Sayed, B. Souloumiac, J.B. Leblond, and J.M. Bergheau. Recent advances in residual stress simulation caused

by the welding process. In *Computational Plasticity XIII - Fundamentals and Applications, ISBN 978-84-944244-6-5, International Center for Numerical Methods in Engineering*, pages 771–782, Barcelona-Spain, September 2015.

[43] J.B. Leblond. Mathematical modelling of transformation plasticity in steels II: Coupling with strain hardening phenomena. *Int. J. Plasticity*, 5(6):573–591, 1989.

[44] D.N. Arnold, F. Brezzi, and M. Fortin. A stable finite element for the stokes equations. *Calcolo*, 21(4):337–344, December 1984.

[45] E. Feulvarch, J.C. Roux, J.M. Bergheau, and P. Gilles. A stable P1P1 finite element for finite strain von Mises elasto-plasticity. *Computer Methods in Applied Mechanics and Engineering*, 324:537–545, September 2017.

[46] E. Feulvarch, R. Lacroix, and H. Deschanels. A 3D locking-free XFEM formulation for the von Mises elasto-plastic analysis of cracks. *Computer Methods in Applied Mechanics and Engineering*, 361:112805, April 2020.

[47] F. Valiorgue. *Simulation des processus de génération de contraintes résiduelles en tournage du 316L. Nouvelle approche numérique et expérimentale*. PhD thesis, Ecole Nationale Supérieure des Mines, Saint-Etienne, 2008.

[48] S. Morville. *Modélisation multiphysique du procédé de Fabrication Rapide par Projection Laser en vue d'améliorer l'état de surface final*. PhD thesis, Bretagne-Sud University, 2012.

[49] J. Goldak, A. Chakravarti, and M. Bibby. A new finite element model for welding heat sources. *Metallurgical Transactions B*, 15(2):299–305, June 1984.

[50] X.S. Gao, C.S. Wu, S.F. Goecke, and H. Kügler. Numerical simulation of temperature field, fluid flow and weld bead formation in oscillating single mode laser-GMA hybrid welding. *Journal of Materials Processing Technology*, 242:147–159, April 2017.